International Journal of Electrical and Computer Engineering (IJECE)
Vol. 11, No. 6, December 2021, pp. 4833~4839
ISSN: 2088-8708, DOI: 10.11591/ijece.v11i6.pp4833-4839

Aiming to the superior of phosphor pattern: Influence of SiO_2 nanoparticles on photoluminescence intensification of YAG:Ce

My Hanh Nguyen Thi[1], Thuc Minh Bui[2], Nguyen Doan Quoc Anh[3]
[1]Faculty of Mechanical Engineering, Industrial University of Ho Chi Minh City, Vietnam
[2]Faculty of Electrical and Electronics Engineering, Nha Trang University, Vietnam
[3]Power System Optimization Research Group, Faculty of Electrical and Electronics Engineering, Ton Duc Thang University, Vietnam

Article Info

Article history:

Received Nov 15, 2020
Revised May 11, 2021
Accepted May 23, 2021

Keywords:

Color uniformity
Luminous flux
Mie-scattering theory
SiO_2

ABSTRACT

Yttrium aluminum garnet (YAG: RE) rare-earth-doped phosphors have great photoluminescence (PL) characteristics and are commonly used in light-emitting rectifying tubes. The RE elements used in these phosphors, however, are precious and in shortage. The production of phosphorus containing a limited amount of RE content is therefore essential. One solution is to manufacture Nano composite phosphors that use an inexpensive and more easily available content as a matrix for RE oxide. In this research, we developed a YAG: Ce/SiO2 Nano composite using a sol-gel procedure; in order to impulse micelle formation and agglomeration, poly (ethylene glycol) and urea have been added, respectively. X-ray diffraction, scanning and transmission electron microscopy (TEM) and energy-dispersive X-ray spectroscopy were used to characterize the Nano composites. In proposing an explanation for this enhancement, we defined the concentration of SiO2 that produced optimum PL enhancement and used geometric models as well as the characterization consequences. Our results demonstrated that a 10% SiO2 concentration produced a 120% PL intensity of pure YAG:Ce. TEM analysis revealed that SiO2 nanoparticles filled the voids between the YAG:Ce crystals' single grain borders, hence inhibiting light scattering, resulting in increased PL. This procedure would be beneficial for the synthesis of low-RE and high-PL phosphors on a wide scale.

Corresponding Author:

Nguyen Doan Quoc Anh
Faculty of Electrical and Electronics Engineering
Ton Duc Thang University
No. 19 Nguyen Huu Tho Street, Tan Phong Ward, District 7, Ho Chi Minh City, Vietnam
Email: nguyendoanquocanh@tdtu.edu.vn

1. INTRODUCTION

As one of the most significant phosphors for white-light-emitting rectifying tubes are rare-earth (RE)-doped yttrium aluminum garnets (YAG: RE) [1]-[3]. RE ions such as Ce and Tb are necessary as doping materials for the preparation of YAG: RE phosphors with strong luminescence particularities. There are, however, a variety of issues with the materials being used, such as the supply of RE materials being impacted by the increasing costs and the export limitations enforced by producing countries. Therefore, it is imperative to create alternative phosphors such as novel phosphors, i.e. RE-free phosphors, 7-10 or nanostructured phosphors (Nano composite phosphors) created to conserve resources by combining RE oxides with affordable materials 11 and 12. SiO_2 nanoparticles are ideal candidates for the RE oxides host matrix towards Nano composite phosphorous materials, since SiO_2 is inexpensive and clear in the visible-

light area and has virtually no effect on the strength of photoluminescence (PL) [4]-[6]. In addition, as a result of the trapping of oxide particles on SiO_2 nanoparticles, PL spectra can be preserved without peak changing. Using a spray-pyrolysis method, Wang *et al.* produced a Gd_2O_3: Eu phosphor comprising SiO_2 nanoparticles. As a result of improved crystallization, this Nano composite phosphor has high luminescence efficiency [7]-[9]. Via a spray-drying process, Mikrajuddin documented the synthesis of stable photo luminescent ZnO colloids in a SiO_2 nanoparticle matrix. While SiO_2 can theoretically improve the performance of phosphorus, the application of SiO_2 nanoparticles to improve the performance of YAG: Ce phosphors have not yet been reported to the best of our knowledge. The first fabrication of YAG: Ce/SiO_2 Nano composite phosphors are reported in this article. The current synthesis was carried out using a modified sol-gel process with additives (a polymer and urea) in comparison to other documented approaches for the synthesis of phosphorous materials requiring specific and complex processes; this method is promising for industrial applications (i.e. direct synthesis and large-scale production). Poly (ethylene glycol) (PEG) induces the forming of micelles in this process, and urea facilitates agglomeration during particle formation [10], [11]. Subsequently, on a huge scale, a YAG: Ce phosphor with a spherical morphology can be directly generated. A thorough investigation was carried out in this research to determine the appropriate amount of SiO_2 nanoparticles needed to achieve the full intensity of PL, and the intensity of PL was compared with that of pure phosphorus YAG. Relied on theoretical considerations, a mechanism for the creation of phosphor particles and light refraction is also proposed.

2. EXPERIMENT

2.1. Preparation of SiO_2-embedded structure

To investigate the effect of SiO_2 nanocomposite on the photoluminescence of YAG:Ce in the LED package, the comparison between our proposed SiO_2-embedded LED configuration and a traditional LED structure (without SiO_2) was conducted. Figure 1 provides the physical model of the simulated WLED. The preparation of SiO_2-embedded WLED structure can be detailed as follows: First, it is necessary to grow an unintentionally doped GaN layer on the original patterned sapphire substrate of the LED. Then, the metal organic chemical vapor deposition (MOCVD) was applied to conventionally develop a GaN layer without doping SiO_2 nanoparticles (u-GaN) on the c-plane PSS. It is noted that this u-GaN layer has a thickness of 3 µm. An interlayer with a thickness of 100 nm using SiO_2 NPs was placed on the u-GaN using plasma-enhanced chemical vapor deposition to create nano-pillars in the GaN film. Before creating the SiO_2 nanopillars into the u-GaN, an etch mask of Ni dot should be prepared by depositing a Ni layer on SiO_2 layer by e-beam evaporation and subsequently 1-minute rapid thermal annealing the combination of Ni, SiO_2 and GaN with N_2 flows at 850ºC. After that, the etching method of inductively coupled plasma was used to etch down the SiO_2 layer into the GaN by 1.5 m with O_2, CF_4 and Cl_2 gases, respectively [12]-[15]. Then after, buffered oxide etchants eliminated the remaining Ni nano-dots on SiO_2 nano-pillars. As a consequence, a GaN prototype was prepared with Nano-pillars arranged vertically. The SiO_2 nanoparticles, which have colloidal diameter of 100 nm, were subsequently filled in the air-void among the pillars on GaN using 5000-rpm spin-coating for 30s. Then, another GaN layer was firmly regrown on these SiO_2 pillars, followed by developing 3-µm thick n-GaN sheet doping silicon. In sequence, a multiquantum-well (MQW) area and a sheet of Mg-doped p-GaN whose thickness is 200 nm were grown [16]-[18]. Here, the Mg-doped p-GaN layer plays a role as a top contact layer of the structure. Also, the traditional u-GaN grown on PSS without using SiO_2 nanocomposite was fabricated for reference and comparison.

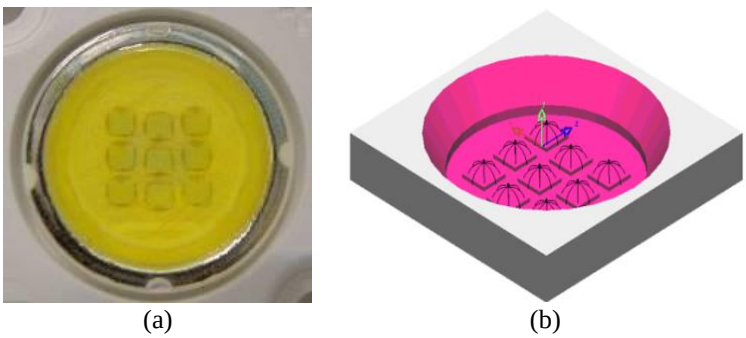

(a) (b)

Figure 1. The physical model of the simulated WLED; (a) photograph of WLEDs sample, (b) the simulated WLEDs model

A field emission scanning electron microscopy (FE-SEM) was used to achieve the cross-section images of the SiO_2 NP LED. The measurements of photoluminescence were carried out at the room temperature, with the excitation source of a 25 mW He-Cd laser at 325 nm line. Indium contact on-wafer testing was applied to determine the properties of current-voltage (I-V) and optical output (L-I). The attained results of the SiO_2 nano-pillar embedded structure were compared with those from the reference model, given that these structures were produced under the same growth conditions. In addition to that, the experimental findings were put into comparison with the results from simulation for a more in-depth analysis. Since the configuration of this experiment and PSS was designed to increase the performance of light extraction for different LED structural designs, the plan is to learn how to achieve better enhancement in the efficiency of the simulation, ensuring that geometric variations are consistent and complementary to each other even though the functions are overlapping.

2.2. Scattering computation

According to Mie-scattering theory [19]-[25], the scattering coefficient $\mu_{sca}(\lambda)$, anisotropy factor $g(\lambda)$, and reduced scattering coefficient $\delta_{sca}(\lambda)$ can be computed by the expressions (1), (2), and (3):

$$\mu_{sca}(\lambda) = \int N(r)\, C_{sca}(\lambda, r) dr \tag{1}$$

$$g(\lambda) = 2\pi \int \int_{-1}^{1} p(\theta, \lambda, r)\, f(r) cos\theta d\, cos\theta dr \tag{2}$$

$$\delta_{sca} = \mu_{sca}(1 - g) \tag{3}$$

where $N(r)$ indicates the distribution density of diffusional particles (mm^3), C_{sca} is the scattering cross sections (mm^2), $p(\theta,\lambda,r)$ is the phase function, λ is the light wavelength (nm), r is radius of diffusional particles (μm), θ is the scattering angle (°C), and $f(r)$ is the size distribution function of the diffusor in the phosphorous layer, which can be calculated as (4), (5):

$$f(r) = f_{dif}(r) + f_{phos}(r) \tag{4}$$

$$\begin{aligned} N(r) &= N_{dif}(r) + N_{phos}(r) \\ &= K_N.\left[f_{dif}(r) + f_{phos}(r)\right] \end{aligned} \tag{5}$$

$N(r)$ consists of $N_{dif}(r)$ and $N_{phos}(r)$, which are densities of the diffusive particles and the phosphor particles, respectively. $f_{dif}(r)$ and $f_{phos}(r)$ indicate the size distribution function data of the diffusive and phosphor particles, in turn. K_N means the number of the diffusor unit for one diffusor concentration which can be expressed by (6):

$$c = K_N \int M(r) dr \tag{6}$$

where M(r) is the mass distribution of the diffusive unit, proposed by (7):

$$M(r) \frac{4}{3} \pi r^3 \left[\rho_{dif} f_{dif}(r) + \rho_{phos} f_{phos}(r)\right] \tag{7}$$

where $\rho_{diff}(r)$ expresses the diffusor's density while $\rho_{phos}(r)$ shows the phosphor crystal's density.

As demonstrated in Mie-scattering theory, the calculation of C_{sca} can be performed as (8):

$$C_{sca} = \frac{2\pi}{k^2} \sum_0^\infty (2n - 1)(|\alpha_n|^2 + |b_n|^2) \tag{8}$$

where $k = 2\pi/\lambda$, with a_n and b_n are computed by (9), (10):

$$\alpha_n(x, m) = \frac{\acute{\psi}_n(mx)\psi_n(x) - m\psi_n(mx)\acute{\psi}_n(x)}{\acute{\psi}_n(mx)\xi_n(x) - m\psi_n(mx)\acute{\xi}_n(x)} \tag{9}$$

$$b_n(x, m) = \frac{m\acute{\psi}_n(mx)\psi_n(x) - \psi_n(mx)\acute{\psi}_n(x)}{m\acute{\psi}_n(mx)\xi_n(x) - \psi_n(mx)\acute{\xi}_n(x)} \tag{10}$$

where $x = k.r, m$ indicates the index of refraction, while $\psi_n(x)$ and $\xi_n(x)$ demonstrate the Riccati-Bessel function.

Therefore, the relative refractive indices of diffusive grains (m_{dif}) and phosphor crystals (m_{phos}) included in the silicone are computed via the following expression: $m_{dif} = n_{dif}/n_{sil}$ and $m_{phos} = n_{phos}/n_{sil}$. Then the phase function can be expressed as (11):

$$p(\theta,\lambda,r) = \frac{4\pi\beta(\theta,\lambda,r)}{k^2 C_{sca}(\lambda,r)} \quad (11)$$

where $\beta(\theta,\lambda,r)$, $S_1(\theta)$ and $S_2(\theta)$ are the angular scattering amplitudes calculated by (12):

$$\beta(\theta,\lambda,r) = \frac{1}{2}[|S_1(\theta)|^2 + |S_2(\theta)|^2] \quad (12)$$

$$S_1 = \sum_{n=1}^{\infty} \frac{2n+1}{n(n+1)} \begin{bmatrix} \alpha_n(x,m)\tau_n(cos\theta) \\ +b_n(x,m)\tau_n(cos\theta) \end{bmatrix} \quad (13)$$

$$S_2 = \sum_{n=1}^{\infty} \frac{2n+1}{n(n+1)} \begin{bmatrix} \alpha_n(x,m)\tau_n(cos\theta) \\ +b_n(x,m)\tau_n(cos\theta) \end{bmatrix} \quad (14)$$

To encapsulate the hydrophobic CdSe-ZnS core-shell QDs with SiO_2, we have established a simple two-step processing path. With this method, Silica-Nano composites containing multiple QDs at incredibly high concentrations have been produced. As a first stage, the spay-drying method was utilized for assembled-QDs preparation. The spray-drying method has also been used to the colloidal nanoparticles' evaporation-assisted self-assembly. During the operation of spray-drying, solvent evaporation causes shrinkage of droplets comprising nanoparticles which are then assembled inside droplets due to capillary force. The aerosol spray method, in particular, significantly enhances solvent evaporation and limits the self-assembly of nanoparticles within the droplet. In reality, different nanoparticles were self-assembled using the aerosol-based spray process to form mesosphere. In this analysis, toluene-dispersed QDs were sprayed ultrasonically at 250 uC for solvent evaporation and hydrophobic QD assembly. The aggregates with high porosity and complex shapes were shaped by the sprayed QDs, and eventually being distributed into hydrophilic ethanol. After being heated at 250 uC for a few seconds, the QDs still retained the surface's hydrophobic quality and could be readily dispersed in toluene. The subsequent adding solution of TEOS and aqueous ammonia resulted in the formation of SiO_2 thin films around spray-dispersed QD aggregates. It is demonstrated that a hydrolytic reaction of TEOS and ammonia attributes to the direct formation 15-nm thick SiO_2 layers on the QDs after a reaction time of 2 hours.

As can be seen in Figure 2, continued response expanded the amount of QD-silica Nano composite particles up to a few micrometers. The temporal evolution of photon emission spectra throughout the growing process of silica nano particles could be seen in Figure 3. Only after the incorporation of TEOS/NH4OH, the QD-silica nano-composite emission intensity was strongly minimized. Some groups have reported that after the formation of QD-silica Nano composite particles, the emission intensity of QDs decreased considerably. The depletion of photoluminescence intensity after the formation of silica layer on the QDs' surface has generally been viewed as the creation of the non-radiative recombination channel. In the synthesis of the QD-SiO_2 nano composite particles, the ligand exchange of silane primer or hydrolyzed TEOS occurred and increase the surface defects, and the non-radiative recombination channel was consequently formed. In general, this partially-hydrolyzed-TEOS rapid ligand exchange caused the TEOS distributed on the surface of QDs to be in a disordered arrangement. Additionally, OH_2 ions can remove the organic ligands on the surface of QDs in aqueous ammonia solution for the TEOS condensation, probably via the creation of hydroxide complexes along with the incomplete surface passivation. Thus, for high photoluminescence pressure, it is advisable to avoid the aqueous ammonia solution's direct reaction. However, since we used an aqueous ammonia solution for the TEOS hydrolysis, as stated by several studies, a gradual decline in emission intensity seems unavoidable.

Several paths, such as initial salinization, and the formation of several shells on QDs, were proposed in an attempt to reduce the photoluminescence-intensity degradation of QDs during the process of forming SiO_2 shell, see Figure 4. The original salinization technique, in specific, has been shown to be successful in maintaining the quantum yield of the original QDs after being encapsulated with SiO_2 Nano composite. Hence, we decided to implement an initial salinization technique in this analysis to reduce the substantial decrease in the intensity of photoluminescence after the creation of SiO_2 layers. In a spray-dispersed QD mixture, 3-aminopropyl-triethoxysilane (APS) was added and reacted for 10 minutes to salinize the QDs under stirring. To thicken the SiO_2 layers, the TEOS and aqueous ammonia solution were added in sequence. Here, after APS addition, the photon emission intensity of the spray-dispersed QD solution was maintained, as shown in Figure 5. And after the addition of TEOS/NH_4OH, the rate of PL displayed only a small

reduction until the reaction time was 1 h. Photoluminescence was weakened by 15-20% as the reaction proceeded further. This result, in fact, is much smaller in comparison with that of the APS-free synthesis. After TEOS/NH_4OH addition, the decrease in PL intensity probably suggests inadequate passivation of the QD surface by APS.

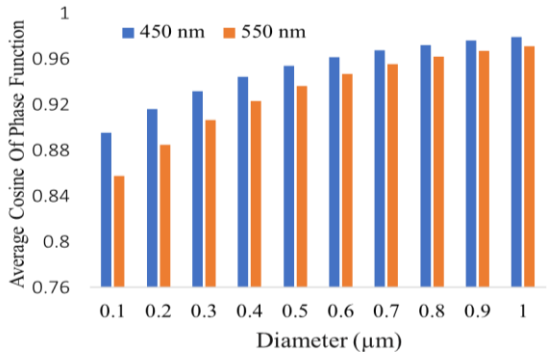

Figure 2. Scattering coefficients of SiO_2 particles at 450 nm and 550 nm

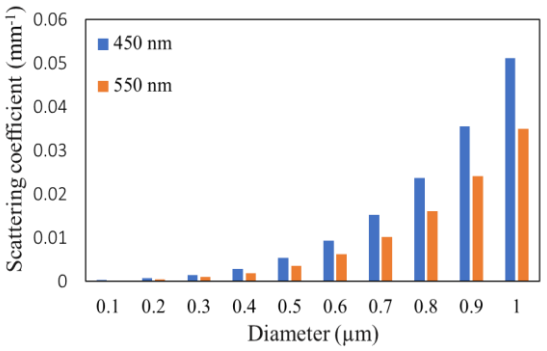

Figure 3. The phase function of SiO_2 particles at 450 nm and 550 nm

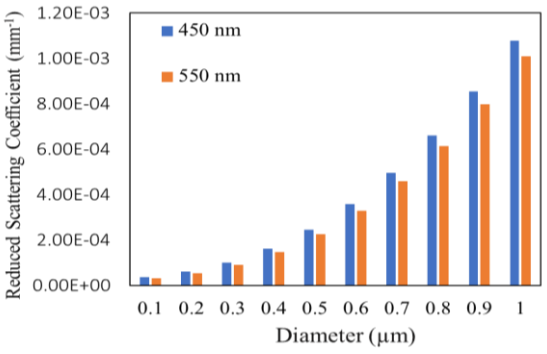

Figure 4. The reduced scattering coefficient of SiO_2 particles at different sizes and wavelength at; (a) 450 nm and (b) 550 nm

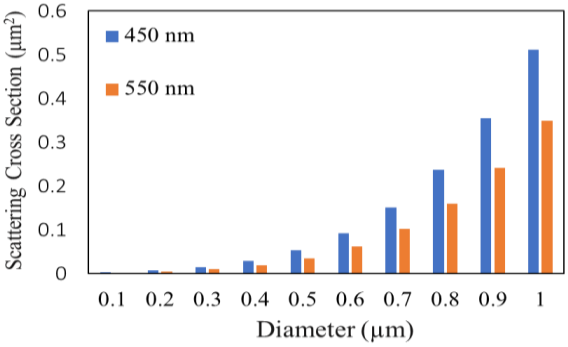

Figure 5. The scattering cross section of SiO_2 particles at different sizes and wavelength at; (a) 450 nm and (b) 550 nm

3. RESULTS AND DISCUSSION

The luminescence changes in connection with different SiO_2 doped contents in the white LEDs packaging structure estimated at 120 mA are shown in Figure 6. Similar forward voltages of all testing instruments are about 3.05 V at 20 mA. Since there are no used antireflection coatings being found in the current paths, there is no effect on the associated electrical properties. Although an anti-reflection covering could be used to widen the critical angle, the reduction in Fresnel reflection was possible to achieve [19]. Moreover, the scattering effect may also be enhanced as the surface of the hybrid SiO_2 microsphere/nanosphere was roughened due to antireflection coating. So, it is possible to further enhance the luminous efficiency of the LED packages. As can be seen from Figure 6, the concentration of used SiO_2 affects the luminous flux of the packages, in which the higher concentration of SiO_2 the better the luminous efficiency. To understand more the luminous property of the SiO_2-doped packages, we utilized the transmission-absorption and haze anlysises to characterize the effects of SiO_2-phosphor-silicone combination for further study. It was pointed out that the enhnacement in the absorption percentage of the SiO_2-intergarted configuration was about 10% (from 32% to 42% approximtely) at 460 nm wavelength, compared to that of the undoped SiO_2 structure. This improvement led to the increase in yellow-light portion in the SiO_2-embbeded packages, thus increasing the lumen output. In this analysis, the effective index would change with the different SiO_2 nanoparticle concentrations after doping the SiO_2 nanoparticle in the phosphorus sheet. In comparison, the silicone, phosphorus and SiO_2 nanoparticle refractive indices (RI) are 1.4, 1.8 and 2.23. The RI of the SiO_2 nanoparticle phosphorous layer is then determined by:

$$RI = V_1RI_1 + V_2RI_2 + V_3RI_3$$

In which, V_1, V_2 and V_3 indicate the concentrations of each materials, including the silicone, the phosphor and SiO_2 nano particle. It is noted that these concentration values are calculated in the weight ratio of the materials. The ratio of SiO_2 concentration to phosphor concentration in the package was 1% wt. and 3% wt. Consequently, the phosphor layer RIs is 1.428 and 1.445 in each layer. A TFCalc32 simulation was used to address the effect of the various refractive index layers. The light extraction value of the SiO_2-nanoparticle dispersed structure is quite close to that of the traditional one, without SiO_2 particle, because of the almost equal refractive index. Therefore, the enhancement of SiO_2 nanoparticle dispensing structure lumen flux could be credited solely to the SiO_2 nanoparticle's dispersing impact. Hence, the scattering effect of SiO_2 particles should be analyzed, and a simulation based on the Mie-scattering theory was conducted for that purpose. In this experimental model, we did not use the yellow phosphor particles, just only the SiO_2 nanoparticles were presented in the packages. This is to reduce the complexity of the structure and the fabrication process. At a wavelength of 460 nm, the refractive index of the SiO_2 with silicone was determined at 2.23. The SiO_2 particle size was roughly 300 nm and the doped concentration of SiO_2 were about 1% and 3% wt., respectively. Before exceeding 500 nm, the haze amplitude of the virtual system structure with a lower SiO_2 dopant content was almost 100 percent and decreased steadily when the wavelength surpassed the mark of 500 nm. We also observed a similarity of the scattering effect of SiO_2 between the experimental results and the simulated results. The haze intensity for doping with a higher SiO_2 content was about the same as for wavelengths ranging from 300 to 700 nm.

The agular correlated color temperature (CCT) deviations of LED packages containing various quantities of SiO_2 nanoparticles were analyzed, and the results were presented in Figure 7. As the instruments were doped with SiO_2 nanoparticles, the consistency of the angle-dependent CCTs was markedly improved. This observation reveals that the increase of the dopant's SiO_2 nanoparticle concentration created a greater scattering impact. The consistency of CCTs in general is indentified as follows: The greatest CCT minus the lowest CCT. The reference CCT was placed at a high level (approximately 5319 K) without doping with SiO_2 nanoparticles, and a higher CCT indicated a higher blue light extraction, which induced a higher CCT variance. The CCT differential found at 00 and 700 was effectively removed when the instruments were doped with SiO_2 nanoparticles. There was a clear impact of SiO_2 doping on phosphorus and silicone on the output of the packed unit.

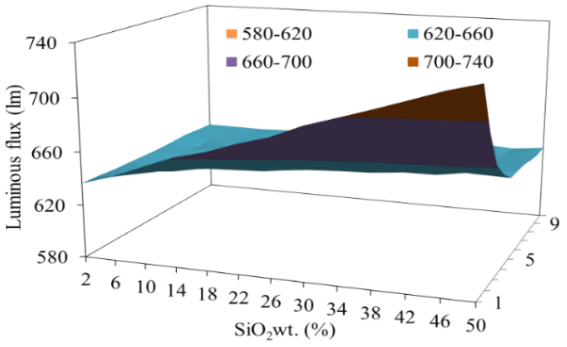

Figure 6. Luminous fluxes of SiO_2 particles with different concentrations

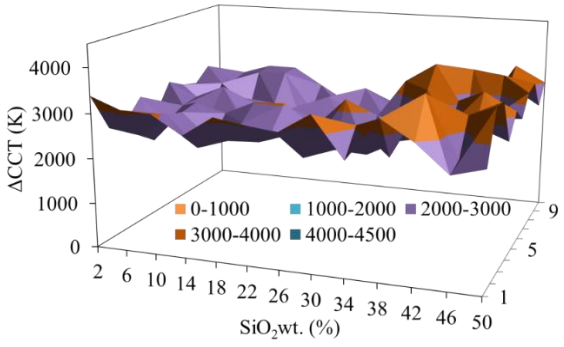

Figure 7. CCT deviations of SiO_2 particles with different concentrations

4. CONCLUSION

In this analysis, by inserting SiO_2 nanoparticles into the precursor solution, the improvement of the PL intensity of a YAG:Ce phosphor was accomplished. The inclusion of SiO_2 nanoparticles decreased the use of costly materials such as Y and Ce, and the composite phosphorus' PL efficiency was higher than that of the pure phosphorus YAG:Ce. The maximum PL intensity at 530 nm was raised to 120% that of a pure YAG:Ce sample by raising the volume of SiO_2. TEM analysis of the YAG:Ce/SiO_2 sample cross-section revealed that SiO_2 filled the voids in the phosphorus sample and blocked the absorption of light at the YAG and SiO_2 interface. We believe that this approach would start to open new and exciting strategies for the synthesis of novel phosphors using lower quantities of costly materials, especially RE materials such as Ce and Y. We also assume that integrating nanoparticle technology with the synthesis of materials would allow RE materials to be used more effectively.

ACKNOWLEDGEMENTS

This research is supported by Industrial University of Ho Chi Minh City (IUH) under grant number 112/HD-DHCN.

REFERENCES

[1] S. Bindai, K. Annapurna, and A. Tarafder, "Realization of phosphor-in-glass thin film on soda-lime silicate glass with low sintering temperature for high color rendering white LEDs," *Applied Optics*, vol. 58, no. 9, pp. 2372-2381, 2019, doi: 10.1364/AO.58.002372.

[2] L. Frey *et al.*, "High-performance silver-dielectric interference filters for RGBIR imaging," *Optics Letters*, vol. 43, no. 6, pp. 1355-1358, 2018, doi: 10.1364/OL.43.001355.

[3] N. C. A. Rashid *et al.*, "Spectrophotometer with enhanced sensitivity for uric acid detection," *Chinese Optics Letters*, vol. 17, no. 8, pp. 081701, 2019.

[4] A. Neitz *et al.*, "Effect of cone spectral topography on chromatic detection sensitivity," *Journal of the Optical Society of America A*, vol. 37, no. 4, pp. A244-A254, 2020, doi: 10.1364/JOSAA.382384.

[5] M. Royer, "Evaluating tradeoffs between energy efficiency and color rendition," *OSA Continuum*, vol. 2, no. 8, pp. 2308-2327, 2019, doi: 10.1364/OSAC.2.002308.

[6] C. Zhang *et al.*, "All-inorganic silicon white light-emitting device with an external quantum efficiency of 1.0%," *Optics Express*, vol. 28, no. 1, pp. 194-204, 2020, doi: 10.1364/OE.382691.

[7] A Correia, P. Hanselaer, and Y. Meuret, "Holistic opto-thermal simulation framework for high-brightness light sources based on fluorescent conversion," *Optics Express*, vol. 27, no. 16, pp. A1324-A1337, 2019, doi: 10.1364/OE.27.0A1324.

[8] Z. Song, T. Guo, X. Fu, X. Hu, "Residual vibration control based on a global search method in a high-speed white light scanning interferometer," *Applied Optics*, vol. 57, no. 13, pp. 3415-3422, 2018, doi: 10.1364/AO.57.003415.

[9] C. S. Kim, W. Kim, K. Lee, and H. Yoo, "High-speed color three-dimensional measurement based on parallel confocal detection with a focus tunable lens," *Optics Express*, vol. 27, no. 20, pp. 28466-28479, 2019, doi: 10.1364/OE.27.028466.

[10] T. Wu *et al.*, "Analyses of multi-color plant-growth light sources in achieving maximum photosynthesis efficiencies with enhanced color qualities," *Optics Express*, vol. 26, no. 4, pp. 4135-4147, 2018, doi: 10.1364/OE.26.004135.

[11] C. Polzer *et al.*, "Correlative two-color two-photon, 2C2P. excitation STED microscopy," *Biomedical Optics Express*, vol. 10, no. 9, pp. 4516-4530, 2019, doi: 10.1364/BOE.10.004516.

[12] P. Zhu, H. Zhu, G. C. Adhikari, and S. Thapa, "Spectral optimization of white light from hybrid metal halide perovskites," *OSA Continuum*, vol. 2, no. 6, pp. 1880-1888, 2019, doi: 10.1364/OSAC.2.001880.

[13] H. Gu, M. Chen, Q. Wang, and Q. Tan, "Design of two-dimensional diffractive optical elements for beam shaping of multicolor light-emitting diodes," *Applied Optics*, vol. 57, no. 10, pp. 2653-2658, 2018, doi: 10.1364/AO.57.002653.

[14] M. K. Kang *et al.*, "Refractive index patterning of infrared glass ceramics through laser-induced vitrification [Invited]," *Optical Materials Express*, vol. 8, no. 9, pp. 2722-2733, 2018, doi: 10.1364/OME.8.002722.

[15] S. Keshri *et al.*, "Stacked volume holographic gratings for extending the operational wavelength range in LED and solar applications," *Applied Optics*, vol. 59, no. 8, pp. 2569-2579, 2020, doi: 10.1364/AO.383577

[16] Y. Wu *et al.*, "Monolithic integration of MoS2-based visible detectors and GaN-based UV detectors," *Photonics Research*, vol. 7, no. 10, pp. 1127-1133, 2019, doi: 10.1364/PRJ.7.001127.

[17] C. Jaques, E. Pignat, S. Calinon, and M. Liebling "Temporal super-resolution microscopy using a hue-encoded shutter," *Biomedical Optics Express*, vol. 10, no. 9, pp. 4727-4741, 2019, doi: 10.1364/BOE.10.004727

[18] H. Yang, H. Bo, L. Zhang, and Y. Yuan, "“Giant” quantum dots encapsulated inside a freeform lens," *Applied Optics*, vol. 57, no. 35, pp. 10317-10322, 2018, doi: 10.1364/AO.57.010317.

[19] S. Jost, C. Cauwerts, and P. Avouac, "CIE 2017 color fidelity index Rf: a better index to predict perceived color difference?," *Journal of the Optical Society of America A*, vol. 35, no. 4, pp. B202-B213, 2018, doi: 10.1364/JOSAA.35.00B202.

[20] B. Xu, Q. Wu, Y. Bao, G. W. Chen, Y. Q. Wang, and S. Ren, "Time-multiplexed stereoscopic display with a quantum dot-polymer scanning backlight," *Applied Optics*, vol. 58, no. 16, pp. 4526-4532, 2019, doi: 10.1364/AO.58.004526 .

[21] B. Jain *et al.*, "High performance electron blocking layer-free InGaN/GaN nanowire white-light-emitting diodes," *Optics Express*, vol. 28, no. 1, pp. 665-675, 2020, doi: 10.1364/OE.28.000665.

[22] C. Su, X. Liu, and J. Zhang, "Analysis of the errors of the integrating sphere for the transmittance of nonplanar optical components," *Journal of Optical Technology*, vol. 85, no. 1, pp. 42-47, 2018, doi: 10.1364/JOT.85.000042.

[23] M. Vanoli, M. Grassi, F. Lovati, S. Barzaghi, T. Cattaneo, and A. Rizzolo, "Influence of innovative coatings on salami ripening assessed by near infrared spectroscopy and aquaphotomics," *Journal of Near Infrared Spectroscopy*, vol. 27, no. 1, pp. 54-64, 2019, doi: 10.1177/0967033518811796.

[24] F. Guan, G. Jiang, Y. Song, M. Yu, Z. Peng, and F. Chen, "No-reference high-dynamic-range image quality assessment based on tensor decomposition and manifold learning," *Applied Optics*, vol. 57, no. 4, pp. 839-848, 2018, doi: 10.1364/AO.57.000839.

[25] P. J. Pardo, M. I. Suero, and Á. L. Pérez, "Correlation between perception of color, shadows, and surface textures and the realism of a scene in virtual reality," *Journal of the Optical Society of America A*, vol. 35, no. 4, pp. B130-B135, 2018, doi: 10.1364/JOSAA.35.00B130.